Determination of Size Distribution and Encapsulation Efficiency of Liposome-Encapsulated Hemoglobin Blood Substitutes Using Asymmetric Flow Field-Flow Fractionation Coupled with Multi-Angle Static Light Scattering

Dian R. Arifin and Andre F. Palmer*

Department of Chemical and Biomolecular Engineering, Center for Molecularly Engineered Materials, University of Notre Dame, Notre Dame, Indiana 46556

In this study, we investigated the size distribution, encapsulation efficiency, and oxygen affinity of liposome-encapsulated tetrameric hemoglobin (LEHb) dispersions and correlated the data with the variation in extruder membrane pore size, ionic strength of the extrusion buffer, and hemoglobin (Hb) concentration. Asymmetric flow field-flow fractionation (AFFF) in series with multi-angle static light scattering (MASLS) was used to study the LEHb size distribution. We also introduced a novel method to measure the encapsulation efficiency using a differential interferometric refractive index (DIR) detector coupled to the AFFF-MASLS system. This technique was nondestructive toward the sample and easy to implement. LEHbs were prepared by extrusion using a lipid combination of dimyristoyl-phosphatidylcholine, cholesterol, and dimyristoyl-phosphatidylglycerol in a 10:9:1 molar ratio. Five initial Hb concentrations (50, 100, 150, 200, and 300 mg Hb per mL of buffer) extruded through five different membrane pore diameters (400, 200, 100, 80, and 50 nm) were studied. Phosphate buffered saline (PBS) and phosphate buffer (PB) both at pH 7.3 were used as extrusion buffers. Despite the variation, extrusion through 400-nm pore diameter membranes produced LEHbs smaller than the pore size, extrusion through 200-nm membranes produced LEHbs with diameters close to the pore diameter, and extrusion through 100-, 80-, and 50-nm membranes produced LEHbs larger than the pore sizes. We found that the choice of extrusion buffer had the greatest effect on the LEHb size distribution compared to either Hb concentration or extruder membrane pore size. Extrusion in PBS produced larger LEHbs and more monodisperse LEHb dispersions. However, LEHbs extruded in PB generally had higher Hb encapsulation efficiencies and lower methemoglobin (metHb) levels. The choice of extrusion buffer also affected how the encapsulation efficiency correlated with Hb concentration, extruder pore size, and the metHb level. The most optimum encapsulation efficiency and amount of Hb entrapped were achieved at the highest Hb concentration and the largest pore size for both extrusion buffers (62.38% and 187.14 mg Hb/mL of LEHb dispersion extruded in PBS, and 69.98% and 209.94 mg Hb/mL of LEHb dispersion extruded in PB). All LEHbs displayed good oxygen-carrying properties as indicated by their P_{50} and cooperativity coefficients. LEHbs extruded in PB had an average P_{50} of 23.04 mmHg and an average Hill number of 2.29, and those extruded in PBS had average values of 27.25 mmHg and 2.49. These oxygen-binding properties indicate that LEHbs possess strong potential as artificial blood substitutes. In addition, the metHb levels in PB-LEHb dispersions are significantly low even in the absence of antioxidants such as *N*-acetyl-L-cysteine.

Introduction

There is an urgent need for universal blood substitutes due to the limited supply of fresh blood, the finite shelf life of blood, and the possibility of infections caused by blood-borne pathogens. Cell-free hemoglobin (Hb) solutions have been evaluated as potential emergency blood substitutes as early as 1943 by Amberson et al. (*1*) and continue to be widely studied even now. There are several types of cell-free Hb solutions: tetrameric Hb composed of two $\alpha\beta$ dimers held together by noncovalent bonds, polymeric Hb produced by intermolecular cross-linking of tetrameric Hb, and conjugated Hb produced by cross-linking individual Hb molecules to polymers (*2*−*6*).

The use of tetrameric Hb as a potential blood substitute was fraught with many problems. The infusion of tetrameric Hb has been shown to induce cytotoxicity, and vasoconstriction (*7*−*9*). Tetrameric Hb is able to extravasate through the capillary walls, where it accumulates in the smooth muscle cells, sequestering NO, which then leads to vasoconstriction. In addition, tetrameric Hb is rapidly filtered and removed by the kidneys, which eventually leads to renal toxicity (*8, 9*). To reduce many of the adverse side effects associated with the use of

10.1021/bp034120x CCC: $25.00
Published on Web 09/09/2003

tetrameric Hb, polymerized Hb based blood substitutes have been developed.

Currently, three polymeric Hbs are in Phase III clinical trials: Hemopure from Biopure Corporation (Cambridge, MA), Polyheme from Northfield Labs (Evanston, IL), and Hemolink from Hemosol, Inc. (Mississauga, ON, Canada). The first two use glutaraldehyde as the cross-linker, and the later uses *o*-raffinose (*3, 4*). Hemospan, a malemide-poly(ethylene glycol) conjugated Hb from Sangart, Inc. (San Diego, CA), is currently undergoing Phase II clinical trial (*4*). These polymeric Hbs have short intravascular circulation half-lives, thus making them most suitable for short-term applications (*2, 3*).

Work is also being done to develop new types of blood substitutes more like erythrocytes by encapsulating Hb inside a semipermeable barrier. Biodegradable nanocapsules composed of polylactide and polyglycolide and liposomes composed of naturally occurring lipids are being explored as potential blood substitutes (*2, 6*). The encapsulated Hb concentration in these systems can be higher or closer to that of erythrocytes (~150 mg of Hb per mL of blood (*10*)). In the case of nanocapsules, proteins and small hydrophilic molecules are able to pass through the polymer membrane, a potential problem not found in liposomes (*2, 11*).

In the case of liposomes, the liposome bilayer acts as an immuno-isolative barrier, which prevents recognition by the reticuloendothelial system, and its size, typically more than 100 nm in diameter, prevents filtration by the capillaries and the kidney microtubules. Liposome-encapsulated hemoglobin (LEHb) has good potential as a universal oxygen carrier since it has no blood group antigens on its surface. It can be readily mass-produced with guaranteed sterility, thus eliminating the possibility of infections and the need to precheck the sterility as in the case of fresh blood. The stability of LEHb for long-term storage is superior compared to fresh blood (*12*). Encapsulating Hb inside phospholipid vesicles permits manipulation of its physiochemical properties and circulation lifetime. Oxidative conversion of the heme group in hemoglobin from the Fe^{2+} form into the Fe^{3+} form, also known as methemoglobin (metHb), can be limited by the presence of the membrane barrier and incorporation of reductants or reductases. Surface modification may increase intravascular persistence and reduce viscosity and aggregation (*7, 8, 12*−*17*). The smaller size of LEHb compared to red blood cells is very advantageous in medical emergencies because it can pass easily through blockages, such as blood clots. In this study, we investigated the size distribution, encapsulation efficiency, and oxygen affinity of LEHb dispersions and correlated these data with the variation in extruder membrane pore size, ionic strength of the extrusion buffer, and Hb concentration.

Various methods of LEHb preparation have been applied in the past years, such as reverse-phase evaporation (*18*), dehydration−rehydration (*19, 20*), detergent dialysis (*21*), extrusion (*17, 22*), and microfluidization (*23*). The last two techniques are gentle on the physical integrity of Hb and will not denature Hb and affect its ability to bind and release oxygen. However, extrusion gives more control over the particle size distribution compared to microfluidization (*22, 23*) and can be readily scaled up for industrial production. With this consideration, we chose extrusion for LEHb preparation.

Because small-diameter LEHb dispersions have been shown to achieve the most optimum circulation lifetime (*24*), it is pertinent to understand the dependence of LEHb size distribution and its oxygen-binding properties on extruder membrane pore size, extrusion buffer, and Hb concentration. To achieve this, we encapsulated tetrameric Hb inside liposomes and measured the differential and cumulative number fraction size distributions of LEHb dispersions using asymmetric flow field-flow fractionation (AFFF) coupled with multi-angle static light scattering (MASLS). Various moments of the size distribution, such as weight-, number-, and z-averages, can be calculated readily from the differential and cumulative number fraction distributions (*25*−*28*).

Many techniques have been used to measure average vesicle size, such as transmission electron microscopy (TEM), sedimentation field-flow fractionation (SFFF), nuclear magnetic resonance (NMR) spectroscopy, gel filtration, and dynamic light scattering. In TEM, the sample has to undergo several preparation steps, which may destroy or alter the sample and introduce artifacts. Moreover, the measurement is done in air or vacuum, not in the sample's original aqueous environment (*29*). SFFF has been proven to be a powerful separation technique, yet a relatively complex centrifugation apparatus is required (*30*). Gel filtration chromatography possesses unsolved limitations, such as limited adsorption range, long elution times, and lipid adsorption to the column (*31*). Dynamic light scattering (*32*) and NMR spectroscopy (*33*) methods are safe toward the sample and can yield accurate measurement of the average particle size. However, prior knowledge of the sample's geometry is required in order to determine the size distribution. Thus, size distribution and particle shape cannot be measured simultaneously and unambiguously. In contrast, classical light scattering or MASLS measurements (*34*) can provide more information about the size and shape of particles in suspension versus dynamic light scattering without prior information on the sample's geometry. The angular distribution of scattered light makes it possible for MASLS to determine the shape (geometry) of particles in solution, the root-mean-square radius of gyration, and the weight-averaged molecular weight of the dispersion. Previous attempts at using dynamic light scattering (DLS) to measure the particle size distribution were performed in batch mode. DLS is most suitably applied to relatively monodisperse samples, or else it will yield misleading information about the particle size distribution. The idea of combining cross-flow FFF with dynamic light scattering has also been explored (*26*). The physical separation of the sample using FFF is followed by collection of each of the eluting fractions and their subsequent analysis in batch mode by dynamic light scattering. In addition to the tedious measurement of each collected fraction, there have been no direct means for measuring the actual particle size of each eluting fraction. Hence, the result has been qualitative at best and has depended critically on the reproducibility of operating conditions.

In addition to economical considerations, high encapsulation efficiencies of Hb are required in order not to overload the patient with lipid (*7*). Hence, an accurate method of quantifying Hb encapsulation is critical. In this study, we outline a novel technique for measuring LEHb encapsulation efficiency. In this extension of our AFFF-MASLS technique, a differential interferometric refractive index (DIR) detector is coupled to the eluent stream of the AFFF-MASLS setup. The DIR signal measures the concentration of the eluting unencapsulated Hb, which is separated from the encapsulated Hb suspension. From this measurement, the encapsulation efficiency can be calculated. The most common method for determining the encapsulation efficiency relies on (*20, 35, 36*) disrupting

the liposome bilayer using the detergent octyl-β-D-glucopyranoside (OBG), before quantifying the Hb content photometrically. This process exposes Hb to detergent, which denatures the Hb, and also led to the incomplete removal of turbidity (*19*). Since it was assumed that the volume of the lipid membrane was negligible compared to the whole volume, this approach overestimated the encapsulation efficiency (*36*). Brandl et al. (*19*) introduced a method to determine encapsulation efficiency without permeabilizing the lipid bilayer of the liposome. Unentrapped Hb was first removed by size exclusion chromatography on Ultragel columns, the unentrapped Hb was then quantified photometrically, and thus the entrapped Hb could be calculated. To quantify the lipid content, the lipid was radiolabeled with ^{14}C and quantified using a scintillation counter. Although this technique was used to overcome the weakness of the first method, Brandl et al. (*19*) mentioned that the photometric assay correction for solution turbidity was not applicable in the case of LEHb dispersions. Farmer et al. (*15*) proposed another technique, which required centrifuging the LEHb suspension and approximating the entrapped Hb concentration by multiplying the Hb concentration in the aliquot with the percent hemocrit. However, this method assumed that the volume of lipids and the interliposomal spaces were negligible and led to underestimation of the encapsulated Hb concentration. Our technique does not require detergents or sample-altering chemicals and corrections for turbidity. In this study, we show that the AFFF-MASLS-DIR technique is an accurate and convenient method for measurement of encapsulation efficiency compared to previous methods. We will also show that encapsulating Hb inside phospholipid vesicles will not compromise the oxygen-carrying potential of Hb solutions as indicated by the physiologically similar P_{50} and cooperativity coefficient of LEHb dispersions.

Materials and Methods

Materials. Dimyristoyl-phosphatidylcholine (DMPC), dimyristoyl-phosphatidylglycerol (DMPG), cholesterol, and polycarbonate membranes were purchased from Avanti Polar Lipid, Inc. (Birmingham, AL). Phosphate buffered saline (PBS) and phosphate buffer (PB) at physiological pH 7.3, were made using phosphate salts and NaCl obtained from Sigma-Aldrich (St. Louis, MO). Spectra/Por cellulose ester dialysis bags with 100,000 MW cutoffs were purchased from Spectrum Laboratories, Inc. (Rancho Dominguez, CA). HEMOX-solution, Additive-A, and anti-foaming agent were purchased from TCS Scientific Corp (New Hope, PA). Octyl-β-D-glucopyranoside (OBG) was obtained from Sigma-Aldrich.

Hb Preparation. Tetrameric Hb solution was obtained from freshly extracted bovine erythrocytes and assayed using a UV−visible spectrophotometer (Varian, Inc., Palo Alto, CA) according to the literature (*37*, *38*). A previous study has shown that bovine Hb is a compatible and convenient replacement of human Hb (*39*). Bovine erythrocytes were extracted, centrifuged, and collected in 3.8% sodium citrate by Animal Technologies, Inc. (Tyler, Texas). To extract Hb from the red blood cells (*38*), erythrocytes were mixed with an equal volume of ice-cold 1.6% sodium chloride solution and centrifuged at 5,000 rpm for 20 min. The supernatant was discarded, and the procedure was repeated twice. The packed erythrocytes were mixed with an equal volume of ice-cold deionized water and shaken for several minutes to lyze the cells. The solution was mixed with ice-cold toluene (20−25% of the total volume of Hb solution), shaken for several minutes, and then left in separatory funnels overnight at 2−3 °C. Cell debris was trapped in the organic layer, and Hb was present in the aqueous layer. The next day, the organic layer was discarded, and the aqueous layer was centrifuged for 1 h at 20,000 rpm. The light colored cell debris was removed, and the Hb solution was filtered through a 0.22-μm Corning cellulose acetate membrane (Fisher Scientific, Pittsburgh, PA). To quantify the Hb concentration (*37*), the solution was diluted to 10 mg/mL (Solution A) with deionized water, and the absorbance was measured at 630 nm (L_1) against a blank reference (deionized water). One drop of KCN solution (1 part 10% KCN and 1 part 0.05 M phosphate, pH 7.6) was added to 1 mL of the solution and mixed. This converted methemoglobin to cyanomethemoglobin, which did not absorb at 630 nm. After 2 min, the absorbance was read at 630 nm against a blank reference (L_2). One milliliter of solution A was diluted with 9 mL of deionized water and mixed with one drop of 20% potassium ferricyanide. After 2 min, one drop of 10% KCN was added. The mixture was measured at 540 nm against a reference consisting of 10 mL of water and one drop each of 20% potassium ferricyanide and 10% KCN (L_3). The concentration of metHb and Hb were calculated using these formulas (*37*, *38*):

$$[\text{metHb}]\ (\text{mM}) = \frac{L_1 - L_2}{3.7} \times \text{dilution factor of solution A} \quad (1)$$

$$[\text{total Hb}]\ (\text{mM}) = \frac{L_3}{11} \times \text{dilution factor of solution A} \times 10 \quad (2)$$

The purity of extracted tetrameric Hb was established by two procedures: AFFF-MASLS-DIR measurement of tetrameric Hb showed a single peak due to tetrameric Hb (PBS pH = 7.3 mobile phase) and size exclusion chromatography under dissociating condition (0.5 M $MgCl_2$ mobile phase) gave rise to one peak corresponding to $\alpha\beta$ dimers.

Lipid Combination. On the basis of a previous study (*15*), a combination of dimyristoyl-phosphatidylcholine (DMPC), cholesterol, and dimyristoyl-phosphatidylglycerol (DMPG) was used in a 10:9:1 mole ratio to produce LEHbs. Unsaturated phosphatidylcholine (PC) was shown (*15*) to oxidize encapsulated Hb in a few days, therefore saturated PC, DMPC in this study, was found to be most suitable. Cholesterol was added to LEHb to overcome several known problems. Intravascularly, cholesterol in erythrocytes membranes transferred to pure phospholipid liposomes membranes as a result of the cholesterol concentration gradient, resulting in osmotically fragile erythrocytes. Addition of cholesterol to liposomes reduced the concentration gradient. Moreover, cholesterol enhanced the liposomes' resistance to fusion and lysis and liposomes' impermeability to small ions. DMPG was included to impart negative charge to the vesicles because neutral liposomes composed of phospholipid and cholesterol had a tendency to aggregate. Moreover, it was shown (*15*) that DMPG was safe when infused into mice and that addition of DMPG in the amount of 5% molar fraction produced the most optimum encapsulation efficiency.

LEHb Preparation. Liposomes were prepared via extrusion. Five initial Hb concentrations (50, 100, 150, 200, and 300 mg Hb per mL of buffer) were extruded through polycarbonate membranes with the following pore diameters: 400, 200, 100, 80, and 50 nm. Twenty

milligrams of the lipid mixture was dried using a Buchi R-205 rotary evaporator (Buchi Analytical, Inc., New Castle, DA) for at least 4 h at 40 °C (*25*). The resultant lipid film was rehydrated with 1 mL of Hb solution of desired concentration (diluted in either PB or PBS at pH = 7.3, accordingly). Extrusion was done in steps starting from a larger pore diameter successively down to the final pore diameter (*15*). Ten passes were executed for each successive step, and 25 passes were done at the final step to achieve a monodisperse dispersion. Empty liposomes were extruded in both PB and PBS to serve as controls.

Size Distribution and Encapsulation Efficiency. LEHb size distributions and encapsulation efficiencies were measured simultaneously using an Eclipse asymmetric flow field-flow fractionator coupled in series to a 18-angle Dawn EOS multi-angle static light scattering photometer, equipped with a linearly polarized 30-mW gallium-arsenide laser operating at 690 nm, and an Optilab DSP differential interferometric refractometer (Wyatt Technology Corp., Santa Barbara, CA). Light scattering spectra were analyzed using the ASTRA software (Wyatt Technology Corp.). The mobile phase for all experiments was PBS at physiological pH = 7.3, filtered through 0.2-μm filters.

Oxygen Affinity. Freshly extruded LEHb was dialyzed overnight in PBS (pH 7.3) at 2−3 °C using dialysis bags with a 100,000-Da molecular weight cutoff (Spectrum Labs, Rancho Dominguez, CA) to separate unencapsulated Hb from the LEHb suspension. In preparation for oxygen-binding measurements, 0.5 mL of dialyzed LEHb was lightly mixed with 4.5 mL of HEMOX solution, 20 μL of Additive-A, and 10 μL of anti-foaming agent. The P_{50} and cooperativity coefficients of LEHb dispersions were measured using a Hemox-Analyzer from TCS Scientific Corp (New Hope, PA) at 37 °C. The P_{50} and cooperativity coefficients were both calculated by fitting the oxygen-binding curve to the Adair equation (*40*).

MetHb Level. Protein adsorption to phospholipid membranes confers resistance to detergent lysis, and octyl-β-D-glucopyranoside (OBG) is the only detergent known to transform LEHb dispersions into micelles (*15*). To measure the MetHb level inside the LEHb dispersion, first freshly extruded LEHb was dialyzed overnight in PBS (pH 7.3) at 2−3 °C, using dialysis bags with 100,000-Da molecular weight cutoff (Spectrum Labs, Rancho Dominguez, CA) to separate the unencapsulated Hb from the LEHb. The dialyzed LEHb, free of unencapsulated Hb, was then vigorously mixed with OBG at a concentration slightly above its critical micellar concentration (30 mg/mL) at room temperature to lyze the liposomes. The encapsulated metHb concentration was measured with UV−visible spectrophotometry (Varian, Inc.) according to the method described above (*38*). In this case, deionized water was replaced with PBS buffer. The total concentration of entrapped Hb in the dispersion volume was calculated by multiplying the encapsulation efficiency with the initial Hb concentration. Spectrophotometry was not used to measure the entrapped Hb concentration, since we found that our procedure to measure encapsulation efficiency was more accurate. However, we had not yet established a better procedure to measure the metHb level (the procedure to measure encapsulation efficiency will be presented later). The metHb level was readily calculated using the following formula (*38*):

$$\text{MetHb level (\%)} = \frac{\text{[MetHb] (mM)}}{\text{[total entrapped Hb] (mM)}} \times 100 \quad (3)$$

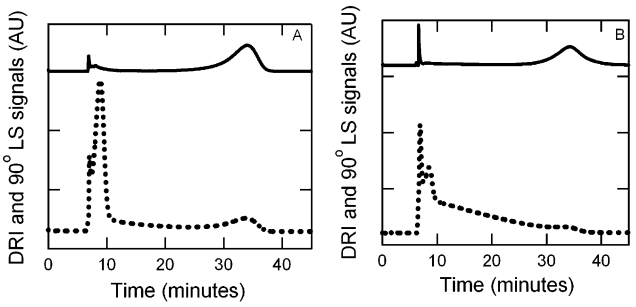

Figure 1. Staggered chromatograms of the differential refractive index (- - -) and the 90° light scattering signals (—) for LEHb made with an initial Hb concentration of 200 mg Hb/mL, extruded through a 100-nm pore diameter membrane. (A) PB as the extrusion buffer, (B) PBS as the extrusion buffer.

Theoretical Background

Light Scattering Theory. During a typical experiment, the sample was first separated on the basis of particle size using the AFFF system. The resultant eluent was then sent through the flow cell of the MASLS photometer, which continuously measured the particles' Raleigh ratio at 16 angles. The eluent subsequently went through the flow cell of the DIR index detector, which continuously measured the molecules' refractive index. A typical chromatogram using the 90° light scattering signal and differential refractive index is shown in Figure 1 (200 mg Hb/mL initial Hb concentration, and 100-nm membrane pore diameter). The first peak corresponds to unencapsulated Hb, and the second peak to the LEHb. The chromatogram shows a distinct separation between the unencapsulated Hb and the LEHb.

In the fractionator system, the channel flow was run parallel to the polymer membrane, while the cross-flow was perpendicular to the membrane. The AFFF channel was preequilibrated by initiating a cross-flow of 3 mL/min, and a channel flow of 0 mL/min for a total of 3 min. During the focus-inject mode of operation, the sample was injected into the channel, where it was subjected to a cross-flow of 3 mL/min and a channel flow of 0 mL/min for 3 min. Particles exposed to the cross-flow accumulated toward the membrane surface, where they rapidly equilibrated via molecular diffusion into a thin ellipsoidal sample front. Instead of diluting our sample, we manipulated injection time (with the injection flow rate set at 0.1 mL/min) to achieve the most optimum light scattering and refractometer signals. The injected football-shaped sample volume was then reduced by applying a cross-flow of 3 mL/min and a channel flow of 0 mL/min for 3 min. After this last focusing step, elution of the sample begun, and the ellipsoidal sample region was exposed to a channel flow of 1 mL/min and a cross-flow, which was linearly decreased from 1 to 0 mL/min over a 30 min interval. The elution was continued for another 10 min without cross-flow. The cross-flow imposes a Stokes drag force that impinges the particles against the channel wall. The effect of the cross-flow on the particles elution time is dependent on the diameter of particles. The drag on the smaller particles is less and their Brownian motion is greater, thus they tend to elute first from the fractionator. This behavior is characterized by an exponential distribution of particles near the accumulation wall (membrane). The particles elution time, t_R, depends on v_c (channel flow velocity), v_x (cross-flow velocity), the channel width, w, and the particle diffusion coefficient, D_v via the following equation (*25*−*28*):

$$t_R \approx \frac{w^2 \nu_x}{6 D_v \nu_c} = \frac{\pi \eta w^2 \nu_x}{2kT\nu_c} d \tag{4}$$

where η is the solvent viscosity, k is Boltzmann's constant, T is the temperature, and d is the particles' diameter. Since the particle's diffusion coefficient is inversely proportional to the particle's diameter, the retention time is directly proportional to the particle's diameter.

In the MASLS flow mode of operation, the data from 16 detectors at the highest angles are used. The light scattering intensity profile is recorded as a function of time at a rate of one full spectra every 1 s. In this paper, the time it takes to collect one complete spectra will be called a slice. Here (*32*),

$$q = \frac{4\pi n}{\lambda_0} \sin\left(\frac{\theta}{2}\right) \tag{5}$$

is the amplitude of the scattering wave vector, $n = 1.3316$ is the refractive index of the buffer solution, θ is the scattering angle, and $\lambda_0 = 690$ nm is the wavelength of the incident light beam in a vacuum.

The excess Rayleigh ratio, $R(\theta)$, describes the light scattered by a sample at a particular angle. The following expression represents the scattering due to particles, which is equal to the difference in scattering between the particles in solution and the buffer solution:

$$R(\theta) = r^2\left(\frac{I_\theta - I_{\theta,\text{solvent}}}{I_0 V}\right) \tag{6}$$

Here, r is the distance between the scattering volume and the detector, I_θ is the scattered intensity of the solution, $I_{\theta,\text{solvent}}$ is the scattered intensity of the solvent, I_0 is the intensity of the incident beam, and V is the volume of the scattering medium. This definition of $R(\theta)$ is very robust since it corrects for any stray light present in the scattering volume along with any fluctuations in laser power. The determination of the size of a monodisperse system of particles can be derived from the following expression proposed by Zimm (*41*, *42*) for a vertically polarized monochromatic light source:

$$\frac{R(\theta)}{Kc} = MP(\theta) - 2A_2 c M^2 P^2(\theta) \tag{7}$$

where

$$K = 4\pi^2 n^2 \frac{\left(\frac{dn}{dc}\right)^2}{\lambda_0{}^4 N_A} \tag{8}$$

K is the optical constant of the hemoglobin solution, N_A is Avogadro's number which is equal to 6.023×10^{23}, c is the mass concentration of hemoglobin in solution, M is the molecular weight of the solute, $P(\theta)$ is the theoretically derived form factor which is a function of the size, shape, and structure of the particle, and A_2 is the second virial coefficient. Since Zimm's expression only takes into account single contacts between macromolecules, it is typically used to model particle scattering in dilute solutions.

To measure the size and shape of particles, values of K and c are not needed; instead eq 7 can be normalized with the light scattering intensity of the 90° detector to yield

$$\frac{R(\theta)}{R(90°)} \approx \frac{P(\theta)}{P(90°)} \tag{9}$$

This equation is used to regress characteristic dimensions of scatterers from experimental light scattering data. For our control, which were empty liposomes, the shape factor for an infinitely thin spherical shell is used:

$$P(\theta) = \left[\frac{\sin qR}{qR}\right]^2 \tag{10}$$

where R is the liposome radius. For LEHb dispersions, the shape factor of a solid sphere is used:

$$P(\theta) = \left[\frac{3}{q^3 R^3}(\sin qR - qR \cos qR)\right]^2 \tag{11}$$

where R is the radius of the sphere.

Figure 2A and B show typical light scattering spectra of LEHbs extruded in PB and PBS, respectively. Although we only show the scattering behavior of LEHb extruded with 100 mg/mL initial Hb concentration, this behavior is typical for similarly sized LEHbs, regardless of the initial Hb concentrations. The solid curves were calculated using the solid sphere model and data from 14 angles. The solid sphere shape factor gives an excellent fit for all sizes except for the LEHb extruded through the 400-nm pore diameter membrane (Figure 2C).

If the molar mass and concentration of each slice comprising the elution peak is known it becomes a trivial process to calculate the following root-mean-square (rms) radius moments for each eluting peak:

Number-average mean square radius:

$$R_n = \frac{\sum\left(\frac{c_i}{M_i}\langle r^2\rangle_i\right)}{\sum\frac{c_i}{M_i}} \tag{12}$$

Weight-average mean square radius:

$$R_w = \frac{\sum(c_i\langle r^2\rangle_i)}{\sum c_i} \tag{13}$$

z-average mean square radius:

$$R_z = \frac{\sum(c_i M_i\langle r^2\rangle_i)}{\sum(c_i M_i)} \tag{14}$$

Here c_i, M_i, and $\langle r^2\rangle_i$ represent the mass concentration, molar mass, and mean square radius of the ith slice. In our case, we replaced the mean square radius with the inner radius derived from either the sphere or thin shell model. The degree of polydispersity of the eluting fraction can be easily calculated via either one of the following definitions: R_w/R_n or R_z/R_n. The last expression weights larger particles more than the former.

Knowledge of the hydrodynamic radius of each eluting slice also allows us to calculate both the cumulative and differential size distribution. The weight fraction of sample having a mean square radius less than $\langle r^2\rangle$, $W(\langle r^2\rangle)$, is defined as

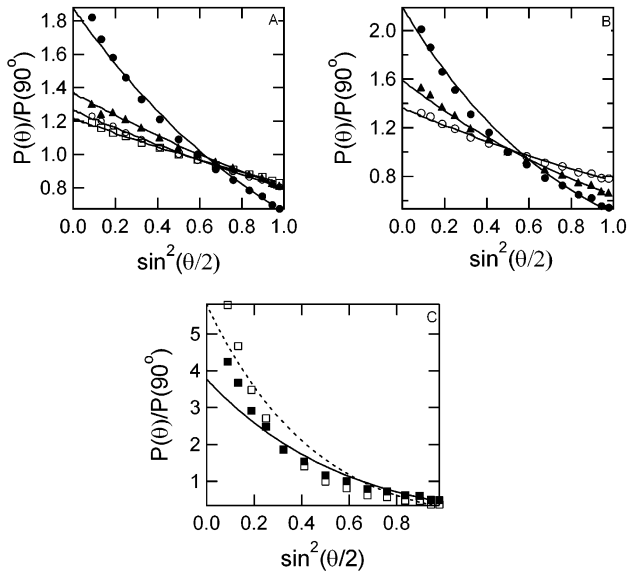

Figure 2. Debye plots of LEHb made with an initial concentration of 100 mg Hb/mL, normalized by the 90° light scattering signal. (A) PB as the extrusion buffer, (B) PBS as the extrusion buffer. LEHbs extruded through various polycarbonate membrane pore diameters are represented by the following symbols: 200 nm (●), 100 nm (▲), 80 nm (○), and 50 nm (□). Solid lines represent fits to the light scattering data using the shape factor of a solid sphere. (C) LEHb extruded in PB through a 400-nm membrane (■) and its sphere shape factor fit (—); LEHb extruded in PBS of identical pore diameter (□) and its sphere shape factor fit (- - -).

$$W(\langle r^2\rangle) = \frac{\sum_{\langle r^2\rangle' < \langle r^2\rangle} c_{\langle r^2\rangle'}}{\sum_{\text{all}\langle r^2\rangle'} c_{\langle r^2\rangle}} \tag{15}$$

where $c_{\langle r^2\rangle'}$ is the mass concentration of the slice having a mean square radius of $\langle r^2\rangle'$. The differential size distribution is defined as

$$x(\langle r^2\rangle) = \frac{\mathrm{d}W(\langle r^2\rangle)}{\mathrm{d}(\log\langle r^2\rangle)} \tag{16}$$

The differential interferometric refractometer is used to measure the change in refractive index of the hemoglobin solution with respect to the solvent in the ith slice (Δn_i). This can be related to the hemoglobin concentration of the ith slice (c_i) via the differential refractive increment of the solution with respect to the change in solute concentration, dn/dc. Therefore $\Delta c_i = \Delta n_i/(\mathrm{d}n/\mathrm{d}c)$, where $\Delta c_i = c_i$, since the differential refractive index baseline represents pure solvent. At $T = 25$ °C and $\lambda_0 = 690$ nm, we measured a dn/dc of 0.185 mL/g for hemoglobin. Since the refractive index is a strong function of wavelength and temperature, all measurements of dn/dc and static light scattering measurements are performed at the same wavelength and temperature.

To calculate the encapsulation efficiency, we measured the DIR signal of eluting unencapsulated Hb, which had been separated from the LEHb mixture (refer to Figure 1), and the DIR signal of a pure Hb solution of identical Hb concentration, which served as the reference. The fraction of unencapsulated Hb was calculated by dividing the area under the DIR signal curve of the unencapsulated Hb by that of the reference. From these measurements, the encapsulation efficiency was calculated.

Encapsulation Efficiency Theory. Applying the assumption that the area under the unencapsulated Hb DIR peaks is proportional to the unencapsulated Hb concentration, the efficiency can be calculated as follows:

$$\text{encapsulation efficiency (\%)} = \left[1 - \frac{\text{unencapsulated Hb area}}{\text{reference area}}\right] \times 100 \tag{17}$$

The reference used here is a Hb solution of equal Hb concentration. The area under the peak is calculated using Scientist Software (Micromath Scientific Software, Inc., St. Louis, MO) with an error-controlled Runge−Kutta integrator.

A typical staggered chromatogram of free-Hb DIR peaks corresponding to the reference (solid line) and unencapsulated Hb (dotted line) in the LEHb solution (150 mg Hb/mL initial Hb concentration, and 400-nm membrane pore diameter) is shown in Figure 3. The top peak (solid line) corresponds to unencapsulated Hb in the reference sample, and the bottom peak (dotted line) corresponds to the unencapsulated Hb in the LEHb dispersion. It is clear that the reference peak has a larger area under the curve and thus higher free-Hb concentration than the unencapsulated Hb sample peak. The area under the peak is integrated from the point when the peak started until 10 min down the line (refer to Figure 1). If LEHb samples are dialyzed to separate the unencapsulated Hb from the LEHb and then fractionated, no peaks due to unencapsulated Hb are observed. Furthermore, the peak corresponding to LEHb elutes after 30 min from the time the elution is initiated and shows definite separation of the LEHb dispersion from the unencapsulated Hb. The purity of extracted Hb was established earlier (see Materials and Methods section), and hence, we are convinced that no traces of LEHb or contaminants contribute to the unencapsulated-Hb signal.

Adair Equation. The Adair equation is used to calculate the P_{50} and cooperativity coefficient of the LEHb dispersion (*40*). This equation is based on a model describing the sequential binding of oxygen to a molecule with four available binding sites, each with a different equilibrium constant. When the equation is derived with overall Adair constants, each successive equilibrium constant describes adding n molecules of oxygen to deoxyhemoglobin.

The overall stoichiometric equation is represented as

$$\mathrm{Hb} + n\mathrm{O} \leftrightarrow \mathrm{HbO}_n \tag{18}$$

The overall equilibrium expression is given by

$$A_n = \frac{[\mathrm{HbO}_n]}{[\mathrm{Hb}]p^n} \tag{19}$$

where A_n is the Adair constant. Hence, the overall Adair equation is given by

$$Y = \frac{A_1p + 2A_2p^2 + 3A_3p^3 + 4A_4p^4}{4(1 + A_1p + A_2p^2 + A_3p^3 + A_4p^4)} \tag{20}$$

The experimentally determined oxygen saturation curve is fitted to the Adair equation to regress the Adair constant and cooperativity coefficient, n. The P_{50} is

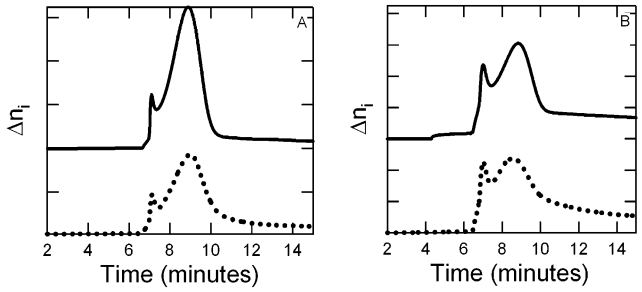

Figure 3. Staggered chromatograms of the differential refractive index of the reference (—) and sample (- - -) of LEHb made with an initial Hb concentration of 50 mg Hb/mL, extruded through a 400-nm membrane. (A) Extrusion in PB, (B) extrusion in PBS.

defined as the partial pressure of oxygen when 50% oxygen saturation is achieved ($Y = 0.5$).

Results and Discussion

Table 1 contains the measured number-average mean square radius (R_n), weight-average mean square radius (R_w), z-average mean square radius (R_z), and polydispersity indices of LEHbs extruded in PB and PBS. Regardless of the initial Hb concentrations, extrusion buffers, and the membrane pore diameters, extrusion through 400-nm pore diameter membranes produced LEHbs smaller than the pore size, extrusion through 200-nm membranes produced LEHbs with diameters close to the pore diameter, and extrusion through 100-, 80-, and 50-nm membranes produced LEHbs larger than the pore size. We found that the resulting radius highly depends on the nature of the lipid combination itself and that LEHbs extruded through pore diameters smaller than 200 nm were unstable, since the liposomes may either aggregate or fuse together to form larger LEHbs or ensemble aggregates. Indeed, this is proven to be an advantage since ~200-nm diameter liposomes were found to have longer vascular retention than 1- to 5-μm diameter liposomes (*2*). The measured radii may appear to be similar despite the variation in entrapped Hb concentration; however, we will prove in the next section that the similarity can be explained by the weak influence of the colloid osmotic pressure due to entrapped Hb on the LEHb size. In Figure 2A and B, we see that LEHbs extruded through 200, 100, 80, and 50 nm exhibit excellent fits to the solid sphere shape factor model (solid lines), indicating that extrusion produces spherically shaped liposomes. However (refer to Figure 2C), the solid sphere shape factor model does not fit well to the largest LEHb (400-nm pore diameter). This is because a significant number of the liposomes are not spherical in shape; hence, we cannot rule out the existence of nonspherically shaped LEHbs. Further study on the morphology of these larger LEHbs will be required to determine their geometry.

Effect of Osmotic Pressure on LEHb Size. The ultimate goal of this work is to infuse LEHbs in live animals or humans as an artificial blood substitute. In this setting, the infused LEHb dispersions will be subjected to physiological osmotic pressures. To mimic this osmotic environment in vitro, we examined the size distributions of our LEHbs in PBS (pH = 7.3). We expect the osmotic pressure to be slightly higher inside PBS-LEHbs as a result of the presence of the encapsulated Hb. In this case, water will diffuse into the liposomes in order to equilibrate the osmotic pressure gradient, which causes the liposomes to slightly swell. The liposomes are impermeable to hydrophilic ions. The swelling could possibly continue in an intravascular setting and cause the LEHb to rupture in vivo. Because of this concern, we also investigated PB as an alternate extrusion buffer. Here, we differentiate between crystalloid osmotic pressure due to electrolytes (K^+, $H_2PO_4^-$, and HPO_4^{2-} in PB with additional Na^+ and Cl^- present in PBS) and colloid osmotic pressure due to entrapped Hb inside the liposomes. The crystalloid osmotic pressure in PB is 2,640.48 mmHg, while that in PBS is 8,520.66 mmHg. The difference between the outside and inside osmotic pressure of PBS-LEHb is only due to the colloid osmotic pressure, whereas in PB-LEHb, both crystalloid and colloid osmotic pressures contribute to the osmotic pressure gradient. The total osmotic pressure gradient (ΔP_{total}) is calculated by subtracting the total osmotic pressure inside the LEHb from the crystalloid osmotic pressure outside the LEHb. Note that because of this, the colloid or the total osmotic pressures of PBS-LEHb ($\Delta P_{colloid}$) are presented as negative values in Table 3. A positive osmotic pressure gradient means that a higher osmotic pressure exists outside of the LEHb and vice versa. The crystalloid osmotic pressure gradient in PB-LEHb is 5,880.19 mmHg and the colloid osmotic pressure ($\Delta P_{colloid}$) is listed in Table 2. We will compare the measured radii of LEHbs extruded in PB versus PBS and concentrate the analysis on the three largest membrane pore radii (200, 100 and 50 nm), since the LEHbs extruded by smaller pore radius membranes aggregate or fuse together to form larger vesicles or aggregates. We find that LEHbs extruded in PB are generally smaller in size than those extruded in PBS, as we have expected. Since the outside osmotic pressure of PB-LEHb is higher, water will diffuse out of the vesicle, resulting in shrinkage, and vice versa, the opposite effect in PBS-LEHb should produce slightly swollen vesicles.

We observed this phenomenon more clearly by concentrating on LEHbs extruded through 100-nm pore radius membranes. The radius of PB-LEHb is 10−20 nm smaller than the pore radius, except at a Hb concentration of 300 mg/mL. In that case, the measured radius is slightly higher. As expected, PBS-LEHb exhibits a radius that is larger than the pore radius by 5−60 nm. Both have larger radii than each respective control, since both have a larger positive osmotic pressure gradient. However, both controls have similar radii, although they have a 5,880.19 mmHg difference in crystalloid osmotic pressure. Furthermore, the osmotic pressure gradient of 100-nm pore radius PBS-LEHb becomes more positive as the Hb concentration decreases (or as the colloid osmotic pressure decreases), even though the measured radius does not decrease as expected. The same behavior is also observed with PB-LEHb.

The change of osmotic pressure gradient in PB-LEHb compared to its control ranges from 30 to 900 mmHg, and between PBS-LEHb and the PBS-control ranges from 5 to 815 mmHg, whereas between the PBS-control and the PB-control it is by far higher, 5,8880.19 mmHg. Moreover, PB-LEHbs are smaller in size than PBS-LEHbs on average but generally have higher encapsulation efficiencies. As we can see in Tables 2 and 3, although the concentration of entrapped Hb is high, the colloid osmotic pressure due to encapsulated Hb has a weak contribution on the total osmotic pressure gradient because it is a large macromolecule (lower osmolarity) and therefore weakly influences LEHb size versus the crystalloid contribution to the total osmotic pressure. We conclude that the ionic strength of the extrusion buffer

Table 1. Various Moments of Size Distributions and Polydispersity Indices of LEHbs Extruded in PB and PBS

		PB as extrusion buffer					PBS as extrusion buffer				
[Hb] (mg/mL)	pore radius (nm)	R_n (nm)	R_w (nm)	R_z (nm)	R_w/R_n	R_z/R_n	R_n (nm)	R_w (nm)	R_z (nm)	R_w/R_n	R_z/R_n
300	200	118.3	119.1	118.7	1.01	1.00	130.1	129.9	129.7	0.59	0.60
	100	101.1	107.4	109	1.06	1.08	117.8	118.6	119	1.01	1.07
	50	85.6	92.4	96.5	1.08	1.13	79.3	80.3	81.1	1.71	1.85
	40	63	61.9	61.9	0.98	0.98	56.3	57.9	59.9	1.58	1.55
	25	47	49.9	52.2	1.06	1.11	50	52.1	53.8	1.88	2.00
200	200	112.3	114.5	115.9	1.02	1.03	139.4	141.6	141.8	0.56	0.57
	100	77.8	79	80.6	1.02	1.04	160.5	160.8	159.8	0.78	0.79
	50	65.5	66.1	68	1.01	1.04	88.4	103.1	109.2	1.31	1.32
	40	52.1	54.2	56.1	1.04	1.08	66.3	67.1	67.7	1.30	1.36
	25	49.7	51.9	53.5	1.04	1.08	90.2	103.2	107.3	1.99	2.08
150	200	128.3	136.4	140.3	1.06	1.09	154.8	159.2	160.8	0.64	0.68
	100	78.3	80.1	81.5	1.02	1.04	105.4	106	106.3	0.78	0.80
	50	85.7	91.5	94.8	1.07	1.11	71.8	73.7	75	1.71	1.83
	40	82.2	88.5	92	1.08	1.12	64.2	71.7	74.7	2.06	2.21
	25	88.9	93.5	96.5	1.05	1.09	53.2	55	56.6	3.56	3.74
100	200	121.5	121.7	121.8	1.00	1.00	137.3	139.6	140.5	0.61	0.61
	100	90.4	91.5	92.2	1.01	1.02	104.2	105.2	105.7	0.90	0.92
	50	59.5	62.1	64	1.04	1.08	81.7	82.7	83.5	1.19	1.24
	40	56	58.1	59.7	1.04	1.07	66.5	67.7	68.6	1.40	1.45
	25	47.1	50.6	53.2	1.07	1.13	53.2	53.4	53.7	1.88	2.02
50	200	134.2	136.9	138.6	1.02	1.03	146.1	147.9	148.9	0.67	0.68
	100	88.9	90.4	91.4	1.02	1.03	109.6	110.5	110.8	0.89	0.90
	50	67.3	69.3	71.2	1.03	1.06	77	77.9	78.6	1.35	1.39
	40	50.6	50.8	52.3	1.00	1.03	62.8	63.8	64.6	1.27	1.27
	25	52.1	53.9	55.6	1.03	1.07	57.1	57.3	57.7	2.08	2.16
0	200	126.3	128.9	129.8	1.02	1.03	125.4	125.8	124.2	1.00	0.99
	100	88.2	88.6	88.5	1.00	1.00	83.2	83.6	83.6	1.00	1.00
	50	67.3	67.1	67	1.00	1.00	75.7	75.6	75.4	1.00	1.00
	40	54.6	54.8	55.1	1.00	1.01	70.3	70.9	71.2	1.01	1.01
	25	51.3	52.2	52.9	1.02	1.03	50.1	53	54.5	1.06	1.09

Table 2. Encapsulation Efficiency, Concentration of Entrapped Hb in LEHb Dispersions, metHb Level, P_{50}, Cooperativity Coefficient, and Osmotic Pressure Gradient of LEHbs Extruded in PB

[Hb] (mg/mL)	pore radius (nm)	encapsulation (%)	Hb entrapped (mg/mL)	Metlevel (%)	P_{50} (mmHg)	Hill no.	$\Delta P_{colloid}$ (mmHg)	ΔP_{total} (mmHg)
300	200	69.98	209.94	24.01	27.15	2.35	914.79	4 965.40
	100	17.49	52.47	3.18	26.03	2.46	228.63	5 651.55
	50	13.83	41.49	51.16	24.81	2.45	180.79	5 699.40
200	200	29.32	58.64	0.00	21.6	2.2	255.52	5 624.67
	100	39.54	79.08	2.52	23.44	2.31	344.58	5 535.61
	50	17.54	35.08	0.04	21.91	2.27	152.86	5 727.33
150	200	48.73	73.10	0.00	20.98	2.17	318.50	5 561.68
	100	33.21	49.82	24.82	22.64	2.31	217.06	5 663.12
	50	34.80	52.20	0.00	22.77	2.38	227.45	5 652.73
100	200	81.31	81.31	0.00	19.01	2.09	354.30	5 525.89
	100	5.12	5.12	0.00	23.74	2.42	22.31	5 857.88
	50	48.61	48.61	5.28	23.39	2.44	211.81	5 668.37
50	200	13.52	6.76	0.00	22.65	2.34	29.46	5 850.73
	100	20.34	10.17	0.00	22.2	2.14	44.31	5 835.87
	50	8.09	4.05	4.12	23.28	1.98	17.63	5 862.56

has the strongest influence on LEHb size compared to either the initial concentration of Hb or the encapsulation efficiency.

Size Distribution of LEHb. The differential and cumulative size distributions of LEHbs extruded in PB and PBS are shown in Figures 4 and 5, respectively. The size distributions of the corresponding controls are shown in Figure 6.

In Figure 4A and B, all LEHb dispersions (extruded in PB) have monodisperse size distributions with an approximate distribution width of 20 nm. Monodisperse distributions are also observed in Figure 5A and B (LEHbs extruded in PBS). The two smallest LEHbs have size distribution widths of 10 nm, whereas the other LEHbs exhibit distribution widths of approximately 20 nm. All differential size distributions in Figure 4A and 5A appear to be Gaussian in nature.

In Figure 4C and D, we observe a highly monodisperse size distribution for PB-LEHbs extruded through 400-nm pore diameter membranes with a distribution width of only a few nm; however, the other pore diameters exhibit wider distributions with widths of approximately 20 nm. If the LEHbs are extruded in the presence of salt, PBS buffer (refer to Figure 5C and D), we notice tighter size distributions across all pore diameters with widths in the 10−20 nm range. For both extrusion buffers, the shape of the size distributions is Gaussian.

As the Hb concentration is increased to 150 mg/mL (Figure 4E and F), most size distributions broaden further and have widths around 40 nm. LEHbs extruded through 200-nm pore diameter membranes exhibit the tightest distribution, with a width of 20 nm. All size distributions are Gaussian in shape, except the distribution attributed to LEHbs extruded through 80-nm pore diameter membranes, and even the distribution of LEHbs extruded through 50-nm pore diameter membranes appears to be slightly skewed. This could have been caused by the aggregation and fusion processes observed in the

Table 3. Encapsulation Efficiency, Concentration of Entrapped Hb in LEHb Dispersions, metHb Level, P_{50}, Cooperativity Coefficient, and Osmotic Pressure Gradient of LEHbs Extruded in PBS

[Hb] (mg/mL)	pore radius (nm)	encapsulation (%)	Hb entrapped (mg/mL)	Metlevel (%)	P_{50} (mmHg)	Hill no.	$\Delta P_{colloid}$ (mmHg)
300	200	62.38	187.14	100	22.36	2.11	−815.44
	100	48.63	145.89	1.63	31.03	2.35	−635.70
	50	37.19	111.57	6.90	35.53	2.85	−486.15
200	200	21.41	42.82	1.49	27.23	2.36	−186.58
	100	21.37	42.74	6.16	26.16	2.24	−186.23
	50	22.14	44.28	9.23	27.82	2.39	−192.94
150	200	10.57	15.86	7.75	27.34	2.31	−69.09
	100	14.85	22.28	14.20	28.92	2.87	−97.06
	50	10.43	15.65	20.03	25.73	2.37	−68.17
100	200	32.58	32.58	3.99	20.85	2.03	−141.96
	100	32.13	32.13	0.03	24.81	2.36	−140.00
	50	22.02	22.02	11.83	23.32	2.46	−95.95
50	200	6.51	3.26	54.50	18.6	2.09	−14.18
	100	5.95	2.98	19.63	19.39	2	−12.96
	50	2.33	1.17	100	22.35	2.03	−5.08

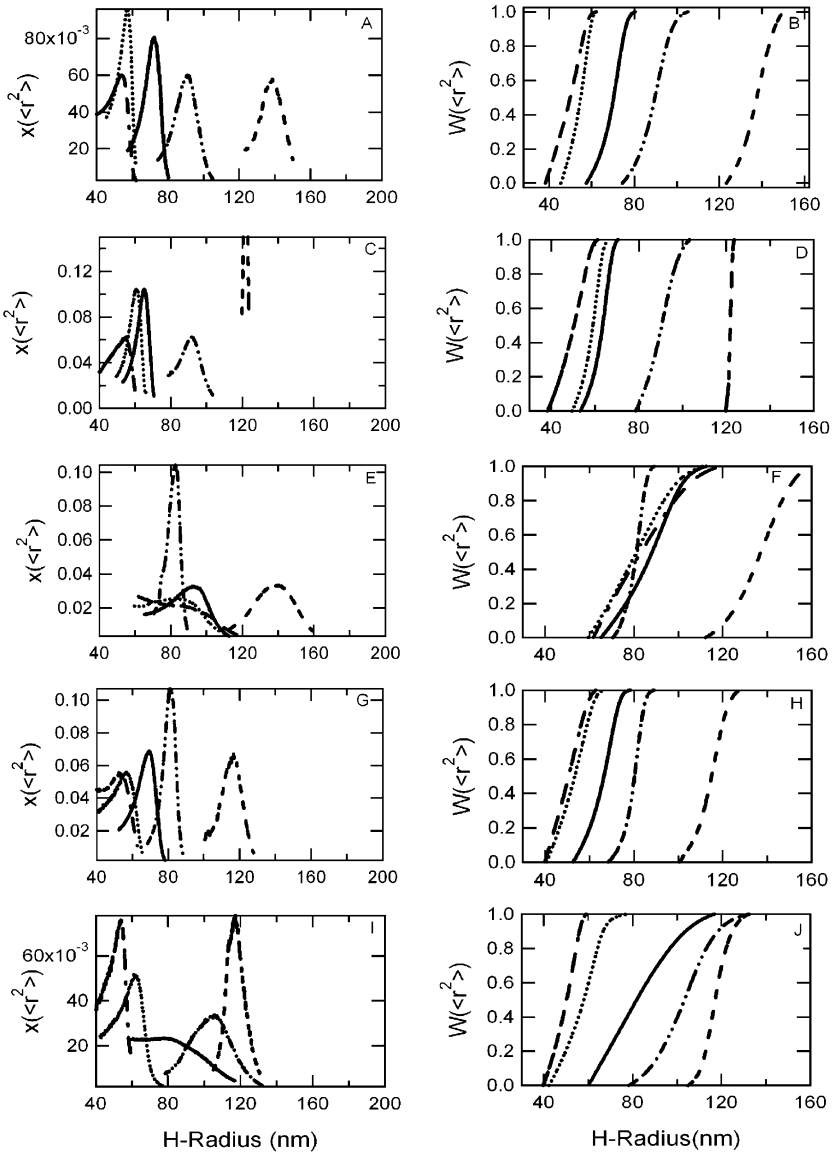

Figure 4. Size distributions of LEHbs extruded in PB buffer. Differential and cumulative number fraction distributions, respectively, of LEHbs made with an initial Hb concentration of (A, B) 50 mg Hb/mL, (C, D) 100 mg Hb/mL, (E, F) 150 mg Hb/mL, (G, H) 200 mg Hb/mL, and (I, J) 300 mg Hb/mL. The following symbols represent the various polycarbonate membrane pore diameters used: 400 nm (- - -), 200 nm (- · · -), 100 nm (—), 80 nm (· · ·), and 50 nm (- · -).

smaller diameter membranes. In the presence of NaCl in the extrusion buffer (Figure 5E and F), the size distributions generally exhibit narrower widths of ∼20 nm, except the 400-nm pore diameter, which had twice the distribution width. Moreover, all size distributions are Gaussian in shape, unlike LEHbs extruded in PB.

All size distributions in Figure 4G and H appear Gaussian with widths in the 20 nm range. However, PB-

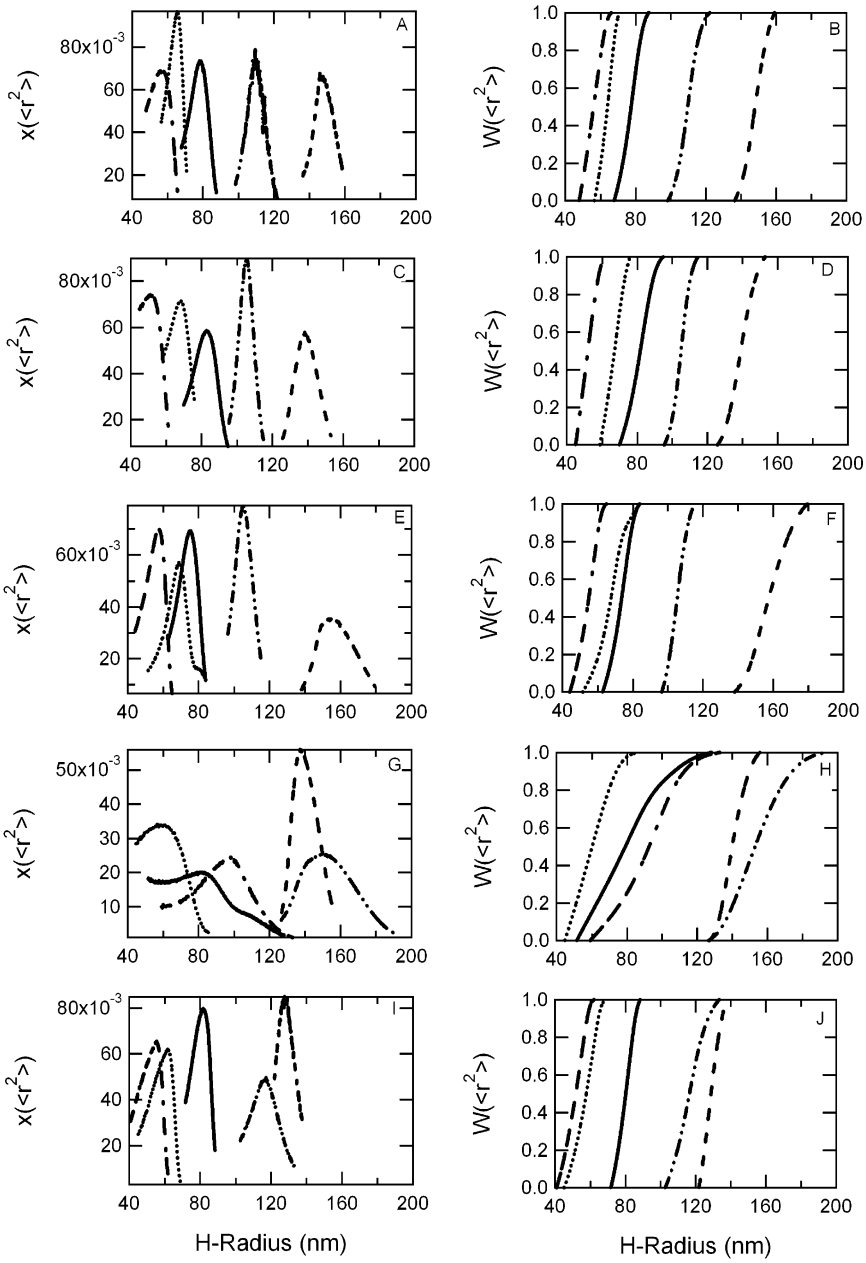

Figure 5. Size distributions of LEHbs extruded in PBS buffer. Differential and cumulative number fraction distributions, respectively, of LEHbs made with an initial Hb concentration of (A, B) 50 mg Hb/mL, (C, D) 100 mg Hb/mL, (E, F) 150 mg Hb/mL, (G, H) 200 mg Hb/mL, and (I, J) 300 mg Hb/mL. The following symbols represent the various polycarbonate membrane pore diameters used: 400 nm (- - -), 200 nm (- · · -), 100 nm (—), 80 nm (· · ·), and 50 nm (- · -).

LEHbs extruded through 400-nm pore diameter membranes exhibit the broadest width of approximately 30 nm. The presence of salt in the extrusion buffer (Figure 5G and H) broadens the size distributions. PBS-LEHbs extruded through 200-nm pore diameter membranes exhibit a distribution width of approximately 20 nm, whereas LEHbs extruded through the other pore diameters have generally wider size distributions with widths ranging from 40 to 55 nm. Although all of them are generally Gaussian in shape, LEHbs produced from 100-nm pore diameter membranes display a slightly skewed distribution.

The highest initial Hb concentration (Figure 4I and J) displays the widest size distribution. LEHbs extruded through a 50-nm pore diameter membranes exhibit a distribution with a width of approximately 20 nm, whereas the others exhibit widths ranging from 40 to 60 nm. All size distributions are Gaussian, except the distribution of LEHbs extruded through 100-nm pore diameter membranes, which is slightly skewed. The size distributions become significantly more monodisperse with the presence of salt in extrusion buffer (Figure 5I and J) and display a Gaussian shape and distribution widths ranging from 10 to 20 nm.

Without Hb encapsulation (Figure 6A and B), the PB-controls exhibit Gaussian shaped curves. Controls extruded through 100- and 200-nm pore diameter membranes have the most monodisperse size distributions with widths of 10 nm, the two smallest sizes (50- and 80-nm pore diameter) exhibit a distribution width of 20 nm, and the largest size (400-nm pore diameter) has the widest size distribution with 40 nm width. PBS-controls also display Gaussian size distributions (Figure 6C and D) with distribution widths ranging from 10 to 20 nm.

In PB-LEHbs, the size distributions slightly broaden as the initial Hb concentration increases. With PBS

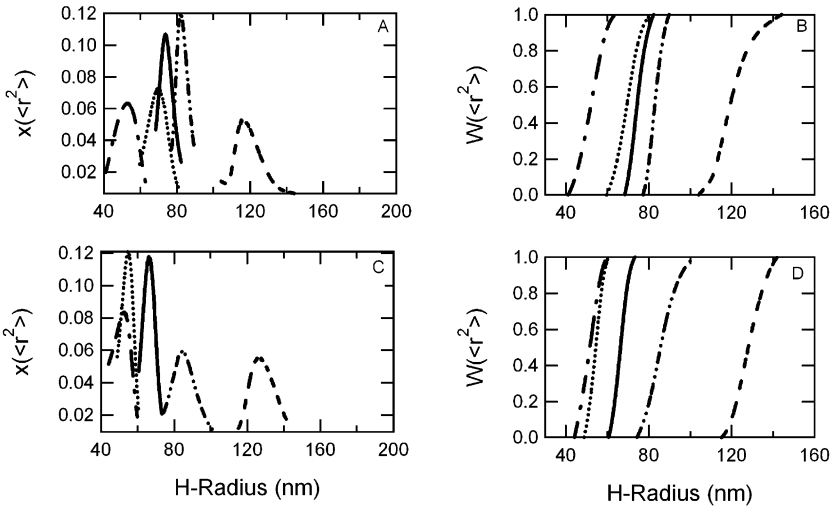

Figure 6. Size distributions of LEHb controls, which are empty liposomes. Differential and cumulative number fraction distributions, respectively, of (A, B) controls extruded in PB and (C, D) controls extruded in PBS. The following symbols represent the various polycarbonate membrane pore diameters used: 400 nm (- - -), 200 nm (- · · -), 100 nm (—), 80 nm (· · ·), and 50 nm (- · -).

extrusion, it is less obvious since the width of the size distributions generally ranges from 10 to 20 nm, except for the 200 mg/mL initial Hb concentration. We conclude that the presence of salt in the extrusion buffer generally results in narrower and more Gaussian-like size distributions, indicating a more homogeneous or monodisperse dispersion.

Sakai et al. (*17*), and Takeoka et al. (*22*) used different phospholipid and cholesterol combinations and employed a Coulter particle analyzer (N4-SD) with a size distribution processor method (SDP) to measure the vesicle size distribution. Sakai et al. (*17*) verified their result using TEM. Their method of LEHb preparation was similar to ours, namely, extrusion with a stepwise reduction of the membrane pore size down to the final pore diameter (Sakai et al. (*17*) used 220 nm as the final pore diameter, while Takeoka et al. (*22*) used 200-nm as the final pore diameter) using PBS as the extrusion buffer. TEM measurements yielded a size distribution of 198 ± 44 nm for Sakai et al. (*17*) (number of LEHbs measured = 55). The N4-SD method yielded a distribution of 251 ± 87 nm for Sakai et al. (*17*) and 200 ± 40 nm for Takeoka et al. (*22*). Unfortunately, we cannot directly compare our results with Sakai et al. (*17*) due to the difference in final pore size, but Takeoka et al. (*22*) reported a similar mean radius with ours for a 200-nm membrane pore diameter (PBS-LEHb) despite having used a different lipid combination. Measuring the LEHb size distribution using either TEM or N4-SD, both groups were not able to obtain differential or cumulative size distributions. The size distribution Sakai et al. (*17*) mentioned was the number of particles versus particles size histogram. Moreover, they also reported a wider size distribution compared to our result (we obtained a standard deviation of 10 nm for PBS-LEHb extruded through 200-nm pore diameter membranes). Mobed and Chang (*43*) measured the size distribution of several lipid combinations (with distearoylphosphatidylcholine and cholesterol as the principal lipids) extruded through a 0.22-μm filter with PBS at pH 7.4 as the extrusion buffer using a DAWN-F multi-angle light scattering photometer in batch mode and reported a mean diameter ranging from 154 to 220 nm.

Identical lipid composition, extrusion buffer, and preparation methods were employed by Farmer et al. (*15*) in characterizing the size of LEHbs extruded through membranes with pore diameters ranging from 3 μm to 200 nm using dynamic light scattering at a 90° angle in batch mode. Farmer et al. reported that the polydispersity (an index of size distribution variability) increased with increasing diameter, but the polydispersity started to level off as the pore diameter reached 200 nm. In contrast, we investigated LEHb sizes in the lower region (50- to 400-nm membrane pore diameters). In our case, the polydispersity indexes do not appear to be influenced by the pore diameters (refer to Table 1), which agrees with Farmer et al.'s observation.

Encapsulation Efficiency. Tables 2 and 3 contain the encapsulation efficiencies and the amount of entrapped Hb in LEHbs extruded in PB and PBS, respectively. Note that the unit of the amount of entrapped Hb should be mg/mL dispersion, since we calculated the values using the total volume of the dispersion. We presented the amount of Hb entrapped in this fashion so that we can compare our data with previous work (*19*). Theoretically, the sodium counter ions mask the charge on the phospholipid, resulting in a decrease in the interlamellar spacing of the multilamellar vesicles formed in the initial hydration step, and thereby decreasing the aqueous trapped volume and encapsulation efficiency (*15, 44*). As predicted, indeed extrusion in PB generally resulted in higher encapsulation efficiencies. Hence, we observe that there is a conflicting effect of the presence of salt in the extrusion buffer with regards to the size distribution and encapsulation efficiency. Extruding with PBS produces monodisperse LEHb suspensions, which had been proven to have a simple exponential clearance kinetics compared to heterogeneous samples (*24*), thus permitting easier control and manipulation of the circulation lifetime. However, extruding with PB produces LEHbs with higher Hb encapsulation.

Our results show that for 300 and 200 mg/mL initial Hb concentrations, the encapsulation efficiencies and amount of Hb entrapped inside LEHbs extruded in PB increase with increasing membrane pore radius until the values reach the membrane pore radius of 100 nm, and then the values start to decrease. This behavior is opposite for the lower initial Hb concentrations. For the lowest three initial Hb concentrations, the encapsulation efficiencies and amount of Hb entrapped inside PBS-LEHbs increase with increasing pore radius until the 100-nm pore radius is reached, and then the values decrease. The values are almost constant for 200 mg/mL initial Hb concentration and increase with increasing

radius for 300 mg/mL. In PB-LEHbs, no correlation is found with respect to the initial Hb concentration. In PBS-LEHbs, the highest encapsulation efficiencies and amount of Hb entrapped are achieved at the highest initial Hb concentration (300 mg/mL), and the lowest are achieved at the lowest initial Hb concentration (50 mg/mL) as we expected. However, a local minimum is achieved at 150 mg/mL and a local maximum at 200 mg/mL, between the two extreme Hb concentrations. For both extrusion buffers, the initial Hb concentration variation has a stronger effect on the encapsulation efficiency, and the amount of Hb entrapped than the pore radius variation.

Brandl et al. (*19*) also studied the effect of initial Hb concentration on encapsulation efficiencies and the amount of Hb entrapped in LEHbs composed of egg phosphatidylcholine and equimolar cholesterol, prepared using the dehydration/rehydration method. They found that between 20 and 60 mg/mL of initial Hb concentration, the amount of encapsulated Hb (mg/mL liposome dispersion) increased while the encapsulation efficiencies (% of total Hb employed) decreased. A plateau in the amount of entrapped Hb was reached above 60 mg/mL, and the optimum encapsulation efficiency occurred at a low concentration of 20 mg/mL. The reported behavior is different than ours, but we should note that Brandl et al. investigated lower initial Hb concentrations and employed LEHbs of different lipid composition and preparation methods. A similar study by Zheng et al. (*20*) on LEHbs prepared by the dehydration/rehydration technique between 5 and 25 wt % (approximately between 52.63 and 263.16 mg/mL) of initial Hb concentration showed a linear correlation between the initial Hb concentration and the encapsulated Hb concentration (wt %). An upper limit to the amount of encapsulated Hb was reached at 25 wt % (approximately 263.16 mg/mL) initial Hb concentration. Zheng et al. reported a mean diameter of 250−300 nm for their dispersion. Even though Zheng et al. employed a different LEHb preparation technique, their observation agrees with our data (PBS-LEHb of 400-nm pore diameter).

Brandl et al. (*19*) reported a phospholipid/entrapped Hb molar ratio of 9797 ± 1218, 1521 ± 164, and 656 ± 241 (10, 20, and 60 mg/mL initial Hb concentration and 2628, 1750, and 788 nm mean diameter, respectively). Using Brandl et al.'s technique (*19*), Sakai et al. (*17*) reported a Hb/lipid weight ratio of 1.61 and Takeoka et al. (*22*) reported a value near 1.7. To better compare our data, we converted the encapsulation efficiencies of 400- and 200-nm membrane pore diameter PBS-LEHbs into the appropriate molar or weight ratios. The phospholipid/entrapped Hb molar ratios of 400-nm pore diameter extruded PBS-LEHbs with 300, 200, 150, 100, and 50 mg/mL initial Hb concentration are 12.31, 53.83, 145.35, 70.75, and 707.05, respectively. The Hb/lipid weight ratios of 200-nm pore diameter extruded PBS-LEHbs with 300, 200, 150, 100, and 50 mg/mL initial Hb concentration are 2.66, 4.01, 2.53, 0.26, and 0.52, respectively. Although Brandl et al. (*19*) employed a different LEHb preparation method and produced bigger LEHb vesicles, their result is comparable with ours. From our previous observation, we expect the phospholipid/entrapped Hb molar ratio to increase (the equivalent of decreasing encapsulation efficiency) with decreasing initial Hb concentration at initial Hb concentrations lower than 100 mg/mL, and we observe this in Brandl et al.'s data. Moreover, the ratio increases with increasing diameter, in similar fashion with previously observed behavior in PBS-LEHbs extruded through a membrane pore diameter larger than 200 nm and an initial Hb concentration lower than 200 mg/mL. Sakai et al. (*17*) used 100 mg/mL as the initial Hb concentration. Although Sakai et al. prepared slightly larger LEHbs (the final extrusion membrane pore diameter was 220 nm), it is also interesting to compare their data with ours. Whereas we obtained 0.26 Hb/lipid weight ratio for identical initial Hb concentrations, Sakai et al. reported a higher value, which indicates higher encapsulation. We have shown earlier that encapsulation decreases with increasing size after reaching a 200-nm pore diameter, but it is possible that the maximum is actually reached at a diameter slightly higher than 200 nm, such as ∼250 nm (the diameter obtained by Sakai et al.). Since Takeoka et al. (*22*) employed extrusion to a final pore diameter of 200 nm, direct comparison with their results is possible. Takeoka et al. used 450 mg/mL initial Hb concentration, and obtained a lower ratio than ours at 300 mg/mL, which agrees with the observation reported by Zheng et al. (*20*).

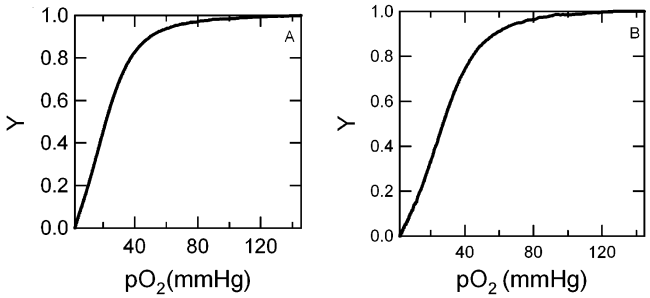

Figure 7. Oxygenation curves of LEHbs made from an initial Hb concentration of 200 mg Hb/mL and extruded through 400-nm membranes. (A) Extrusion in PB and (B) extrusion in PBS.

We have shown that the encapsulation data measured by the DIR technique are comparable with those found in the literature, and hence we can conclude that our new technique provides an accurate and convenient mean of measuring Hb encapsulation.

Oxygen Affinity and Cooperativity Coefficient. The measured P_{50} of pure bovine blood is 25.68 mmHg, and its Hill coefficient, an index of cooperativity of oxygen binding, is 2.46. The result agrees with the values reported in the literature, 26 mmHg (*45*) and 2.4 ± 0.2 (*46*). LEHbs extruded both in PB and PBS possess P_{50} and Hill coefficients close to pure blood values (refer to Tables 2 and 3), indicating that encapsulating Hb in phospholipid vesicles does not compromise Hbs oxygen affinity. The oxygenation curves of LEHbs are shown in Figure 7, PB-LEHbs in panel A and PBS-LEHbs in panel B. Although we only show LEHbs of 400-nm pore diameter and 200 mg/mL initial Hb concentration, Figure 7 represents typical oxygenation curves of LEHb dispersions. Bovine blood responds to chloride ions as its allosteric modifier (*47*). The presence of NaCl in the extrusion buffer slightly shifts the oxygen-binding curve to the right, thus promoting the release of oxygen molecules at higher P_{50}s. In both cases, we find no correlation between the oxygen-binding properties and the initial Hb concentration or membrane pore diameter.

Methemoglobin Level. Tables 2 and 3 contain metHb levels of LEHbs extruded in PB and PBS, respectively. Various groups (*17*, *48*, *49*) have observed that encapsulating Hb inside liposomes enhanced Hb oxidation and increased metHb level. This phenomenon is observed in PBS-LEHbs, but not in PB-LEHbs. PB-LEHbs generally display very low MetHb levels. A quantitative study done by Wallace, et al. (*50*) demonstrated that the anions, in

particular chloride ions, promote the autoxidation of Hb, and this explains the lower metlevel we observed in PB-LEHbs. We find that the initial Hb concentration variation does not influence the metHb level. LaBrake and Fung (*48*) found that small unilamellar vesicles enhanced Hb oxidation more than large unilamellar vesicles. This phenomenon is not observed in our data. MetHb levels of PB-LEHbs are not affected by membrane pore size variation, and PBS-LEHbs exhibited inconclusive or random fluctuations in metHb levels with respect to membrane pore size.

Conclusion

Regardless of the initial Hb concentrations, extrusion buffers, and the membrane pore diameters, extrusion through 400-nm pore diameter produced LEHbs smaller than the pore size, extrusion through 200 nm produced LEHbs with diameters close to the pore diameter, and extrusion through 100, 80, and 50 nm produced LEHbs larger than the pore size. Our observations reveal that LEHb size is mostly determined by the composition of phospholipids and cholesterol in the lipid bilayer, while the ionic strength of the extrusion buffer has a slight influence on LEHb size. In this study, we introduced a novel technique for measuring the encapsulation efficiency using AFFF-MASLS-DRI, which is convenient and nondestructive toward the sample. Upon comparison with previous studies (*17*, *19*, *20*, *22*), we show that our encapsulation data is comparable with previous work, thereby proving that our new technique is accurate and dependable.

Extrusion with PBS produced a more monodisperse and homogeneous LEHb dispersion. In contrast, extruding with PB generally produced liposomes with higher encapsulation efficiencies and lower metHb levels. The choice of buffer also significantly influenced the effect of pore diameter and initial Hb concentration on encapsulation efficiency and the amount of entrapped Hb. Since PBS-LEHbs exhibited high encapsulation efficiencies (62.38% for 300 mg/mL initial Hb concentration extruded through 400-nm pore diameter membranes), and we prefer monodisperse products in a clinical setting, we will choose PBS as the extrusion buffer for future animal studies.

We also measured the oxygen affinity (P_{50} and Hill number) and metHb level of LEHbs. The presence of NaCl in PBS tends to slightly shift the oxygenation curve to the right, increasing the values of P_{50} and Hill coefficient and promoting the release of oxygen at higher P_{50}s, a favorable trait in metabolically active tissues such as muscle (*10*). Both PB-LEHbs and PBS-LEHbs have good oxygen affinities as indicated by their P_{50} and Hill numbers, and hence the choice of extrusion buffer will depend on LEHbs' future application and preference. Nevertheless, we have shown that LEHbs exhibited strong potential as artificial blood substitutes. PB-LEHbs have very low metHb levels, and in contrast, PBS-LEHbs have significant metHb levels. The increased metHb level in PBS-LEHb is expected since we did not suppress Hb oxidation, but the level in PB-LEHbs is surprising. This phenomenon will be explored further as a potential solution to the ongoing problem of high Hb oxidation in LEHbs.

Acknowledgment

We acknowledge support from the National Science Foundation BES-0196432 (Arlington, VA). We would like to thank Denis Birdsell and Rian Galloway from the Center for Environmental Science and Technology (University of Notre Dame, South Bend, IN) for the use of the Center's facilities.

References and Notes

(1) Amberson, W. R.; Flexner, J.; Steggerda, F. R.; Mulder, A. G.; Tendler, M. J.; Pankratz, D. S.; Laug, E. P. On the Use of Ringer-Locke Solutions Containing Hemoglobin as a Substitute For Normal Blood in Mammals. *J. Cell. Comp. Physiol.* **1934**, *5*, 359.

(2) Chang, T. M. S. Future Prospects for Artificial Blood. *Trends Biotechnol.* **1999**, *17*, 61−67.

(3) Moore, E. Blood Subtitutes: The Future is Now. *J. Am. Coll. Surgeons* **2003**, *196*, 1−17.

(4) Chang, T. M. S. Oxygen Carriers. *Curr. Opin. Invest. Drugs* **2002**, *3*, 1187−1190.

(5) Chang, T. M. S. Artificial Cell Biotechnology for Medical Applications. *Blood Purif.* **2000**, *18*, 91−96.

(6) Frietsch, T.; Lenz, C.; Waschke, K. F. Artificial oxygen carriers. *Eur. J. Anaesthesiol.* **1998**, *15*, 571−584.

(7) Riess, J. G. Oxygen Carriers ("Blood Substitutes")-Raison d'Etre, Chemistry and Some Physiology. *Chem. Rev.* **2001**, *101*, 2797−2919.

(8) Rabinovici, R. The Status of Hemoglobin-Based on Red Cell Substitutes. *Reviews* **2001**, *3*, 691−697.

(9) Stowell, C. P. Hemoglobin-Based Oxygen Carriers. *Curr. Opin. Hematol.* **2002**, *9*, 537−543.

(10) Fournier, R. L. In *Basic Transport Phenomena in Biomedical Engineering*; Taylor & Francis: Philadelphia, 1999.

(11) Chang, T. M. C.; D'Agnillo, F.; Yu, W. P.; Razack, S. Two Future Generations of Blood Substitutes Based on Polyhemoglobin-SOD-Catalase and Nanoencapsulation. *Adv. Drug Delivery Rev.* **2000**, *40*, 213-218.

(12) Sakai, H.; Tomiyama, K.; Sou, K.; Takeoka, S.; Tsuchida, E. Poly(ethylene glycol)-Conjugation and Deoxygenation Enable Long-Term Preservation of Hemoglobin-Vesicles as Oxygen Carriers in a Liquid State. *Bioconjugate Chem.* **2000**, *11*, 425−432.

(13) Rudolph, A. S. Encapsulated Hemoglobin: Current Issues and Future Goals. *Artif. Cells, Blood Substitutes, Immobilization Biotechnol.* **1994**, *22*, 347−360.

(14) Rudolph, A. S. Biomaterial Biotechnology Using Self-Assembled Lipid Microstructures. *J. Cell. Biochem.* **1994**, *56*, 183−187.

(15) Farmer, M. C.; Gaber, B. P. Liposome-Encapsulated Hemoglobin as an Artificial Oxygen-Carrying System. *Methods Enzymol.* **1987**, *149*, 184−200.

(16) Takeoka, S.; Sakai, H.; Kose, T.; Mano, Y.; Seino, Y.; Nishide, H.; Tsuchida, E. Methemoglobin Formation in Hemoglobin Vesicles and Reduction by Encapsulated Thiols. *Bioconjugate Chem.* **1997**, *8*, 539−544.

(17) Sakai, H.; Hamada, K.; Takeoka, S.; Nishide, H.; Tsuchida, E. Physical Properties of Hemoglobin Vesicles as Red Cell Substitutes. *Biotechnol. Prog.* **1996**, *12*, 119−125.

(18) Szoka, F.; Papahadjopoulos, D. Procedure for Preparation of Liposomes with Large Internal Aqueous Space and High Capture by Reverse-Phase Evaporation. *Proc. Natl. Acad. Sci. U.S.A.* **1978**, *75*, 4194−4198.

(19) Brandl, M.; Gregoriadis, G. Entrapment of Haemoglobin into Liposomes by the Dehydration−Rehydration Method: Vesicle Characterization and In Vivo Behavior. *Biochim. Biophys. Acta* **1994**, *1196*, 65−75.

(20) Zheng, S.; Zheng, Y.; Beissinger, R. L.; Fresco, R. Microencapsulation of Hemoglobin in Liposomes Using a Double Emulsion, Film Dehydration/Rehydration Approach. *Biochim. Biophys. Acta* **1994**, *1196*, 123−130.

(21) Choquet, C. G.; Patel, G. B.; Beveridge, T. J.; Sprott, G. D. Formation of Unilamellar Liposomes from Total Polar Lipid Extracts of Methanogens. *Appl. Environ. Microbiol.* **1992**, *58*, 2894−2900.

(22) Takeoka, S.; Ohgushi, T.; Terase, K.; Ohmori, T.; Tsuchida, E. Layer-Controlled Hemoglobin Vesicles by Interaction of Hemoglobin with a Phospholipid Assembly. *Langmuir* **1996**, *12*, 1755−1759.

(23) Vivier, A.; Vuillemard, J. C.; Ackermann, H. W.; Poncelet, D. Large-Scale Blood Substitute Production Using a Microfluidizer. *Biomater., Artif. Cells, Immobilization Biotechnol.* **1992**, *20*, 377−397.
(24) Juliano, R. L.; Stamp, D. The Effect of Particle Size and Charge on the Clearance Rates of Liposomes and Liposome Encapsulated Drugs. *Biochem. Biophys. Res. Commun.* **1975**, *63*, 651−658.
(25) Korgel, B. A.; VanZanten, J. H.; Monbouquette, H. G. Vesicle Size Distributions Measured by Flow Field-Flow Fractionation Coupled with Multiangle Light Scattering. *Biophys. J.* **1998**, *74*, 3264−3272.
(26) Wyatt, P. J. Submicrometer Particle Sizing by Multiangle Light Scattering following Fractionation. *J. Colloid Interface Sci.* **1997**, *197*, 9−20.
(27) Wittgren, W.; Wahlund, K. G. Fast Molecular Mass and Size Characterization of Polysaccharides Using Asymmetrical Flow Field-Flow Fractionation-Multiangle Light Scattering. *J. Chromatogr. A.* **1997**, *760*, 205−218.
(28) Roessner, D.; Kulicke, W.-M. On-Line Coupling of Flow Field-Flow Fractionation and Multi-Angle Laser Light Scattering. *J. Chromatogr. A* **1994**, *687*, 249−258.
(29) Egelhaaf, S. U.; Wehrli, E.; Muller, M.; Adrian, M.; Schurtenberger, P. Determination of the Size Distribution of Lecithin Liposomes: A Comparative Study Using Freeze Fracture, Cryoelectron Microscopy and Dynamic Light Scattering. *J. Microsc.* **1996**, *184*, 214−228.
(30) Dreyer, R.; Hawrot, E.; Sartorelli, A. C.; Constantinides, P. P. Sedimentation Field Flow Fractionation of Fused Unilamellar Vesicles: Comparison with Electron Microscopy and Gel Filtration. *Anal. Biochem.* **1988**, *175*, 433−441.
(31) Lesieur, S.; Madelmont, C. G.; Paternostre, M.; Ollivon, M. Study of Size Distribution and Stability of Liposomes by High Performance Gel Exclusion Chromatography. *Chem. Phys. Lipids* **1993**, *64*, 57−82.
(32) VanZanten, J. H. Characterization of Vesicles and Vesicular Dipersions via Scattering Techniques. In *Vesicles*; Rosoff, M., Ed.; Marcel Dekker: New York, 1996; Chapter 7, pp 239−294.
(33) Hinton, D. P.; Johnson, C. S. Diffusion Ordered 2D NMR Spectroscopy of Phospholipid Vesicles: Determination of Vesicle Size Distribution. *J. Phys. Chem.* **1993**, *97*, 9064−9072.
(34) VanZanten, J. H.; Monbouquette, H. G. Characterization of Vesicles by Classical light Scattering. *J. Colloid Interface Sci.* **1991**, *146*, 330−336.
(35) Farmer, M. C.; Rudolph, A. S.; Vandegriff, K. D.; Hayre, M. D.; Bayne, S. A.; Johnson, S. A. Liposome-Encapsulated Hemoglobin: Oxygen Binding Properties and Respiratory Function. *Biomater., Artif. Cells, Artif. Organs* **1988**, *16*, 289−299.
(36) Deshpande, S. V.; Beissinger, R. L. Liposome-Encapsulated Hemoglobin Using Film Hydration Processing to Form Artificial Red Blood Cells. *Biomater., Artif. Cells, Immobilization Biotechnol.* **1993**, *21*, 135−151.
(37) Oser, B. L. In *Hawk's Physiological Chemistry*; McGraw-Hill Book Company: New York, 1965; pp 1096−1968.
(38) DeVenuto, F.; Zuck, T. F.; Zegna, A. I.; Moores, W. Y. Characteristics of Stroma-Free Hemoglobin Prepared by Crystallization. *J. Lab. Clin. Med.* **1977**, *89*, 509−516.
(39) Sakai, H.; Masada, Y.; Takeoka, S.; Tsuchida, E. Characteristics of Bovine Hemoglobin as a Potential Source of Hemoglobin-Vesicles for an Artificial Oxygen Carrier. *J. Biochem.* **2002**, *131*, 611−617.
(40) Voet, D.; Voet, J. G. In *Biochemistry*; John Wiley & Sons: New York, 1995; Chapter 9, pp 241−242.
(41) Zimm, B. H. The Scattering of Light and the Radial Distribution Function of High Polymer Solutions. *J. Chem. Phys.* **1948**, *16*, 1093−1099.
(42) Zimm, B. H. Apparatus and Methods for Measurements and Interpretation of the Angular Variation of Light Scattering; Preliminary Results on Polystyrene Solutions. *J. Chem. Phys.* **1948**, *16*, 1099−1116.
(43) Mobed, M.; Chang, T. M. S. Comparison of Polymerically Stabilized PEG-grafted Liposomes and Physically Adsorbed Carboxymethylchitin and Carboxymethyl/glycolchitin Liposomes for Biological Application. *Biomaterials* **1998**, *19*, 1167−1177.
(44) Hauser, H. Some Aspects of the Phase Behavior of Charged Lipids. *Biochim. Biophys. Acta* **1984**, *772*, 37−50.
(45) Simoni, J.; Simoni, G.; Feola, M. Chromatography Analysis of Biopolymers Distribution in "Poly-Hemoglobin", an Intermolecularly Crosslinked Hemoglobin Solution. *Anal. Chim. Acta* **1993**, *279*, 73−88.
(46) Feola, M.; Gonzalez, H.; Canizaro, P. C.; Bingham, D.; Periman, P. Development of a Bovine Stroma-Free Hemoglobin Solution as a Blood Substitute. *Surg. Gynecol. Obstet.* **1983**, *157*, 399−408.
(47) Fronticelli, C.; Bucci, E.; Orth, C. Solvent Regulation of Oxygen Affinity in Hemoglobin. *J. Biol. Chem.* **1984**, *259*, 10841−10844.
(48) LaBrake, C. C.; Fung, L. W. M. Phospholipid Vesicles promote Human Hemoglobin Oxidation. *J. Biol. Chem.* **1992**, *267*, 16703−16711.
(49) Yoshida, Y.; Kashiba, K.; Niki, E. Free Radical-Mediated Oxidation of Lipids Induced by Hemoglobin in Aqueous Dispersion. *Biochim. Biophys. Acta* **1994**, *1201*, 165−172.
(50) Wallace, W. J.; Maxwell, J. C.; Caughey, W. S. A Role for Chloride in the Autoxidation of Hemoglobin under Conditions Similar to Those in Erythrocytes. *FEBS Lett.* **1974**, *43*, 33−36.

Accepted for publication July 10, 2003.

BP034120X